Applied Catalysis A: General 493 (2015) 112–120

Contents lists available at ScienceDirect

Applied Catalysis A: General

journal homepage: www.elsevier.com/locate/apcata

Post-synthesized zirconium-containing Beta zeolite in Meerwein–Ponndorf–Verley reduction: Pros and cons

Jie Wang[a,1], Kazu Okumura[b], Stephan Jaenicke[a], Gaik-Khuan Chuah[a,*]

[a] Department of Chemistry, National University of Singapore, 3 Science Drive 3, Kent Ridge, Singapore 117543, Singapore
[b] Faculty of Engineering, Department of Applied Chemistry, Kogakuin University, 2665-1 Nakano-machi, Hachioji City, Tokyo 192-0015, Japan

ARTICLE INFO

Article history:
Received 21 October 2014
Received in revised form
22 December 2014
Accepted 4 January 2015
Available online 10 January 2015

Keywords:
Zirconium-beta
Zeolite
Post-synthesis
Lewis acidity
Meerwein–Ponndorf–Verley reduction

ABSTRACT

Zr-Beta zeolite was prepared by a two-step post-synthesis method involving dealumination of Al-Beta followed by wet impregnation with $Zr(NO_3)_4$. Compared with Zr-Beta formed under fluoride-mediated hydrothermal conditions, the post-synthesized samples had smaller particle size and stronger Lewis acidity. The materials were tested as catalysts for Meerwein–Ponndorf–Verley reduction. In the reduction of 4-*tert*-butylcyclohexanone, it exhibited the same excellent stereoselectivity toward *cis*-4-*tert*-butylcyclohexanol (>99%) as the HF-synthesized Zr-Beta, but had a lower TOF. Because of the higher density of zirconium sites and the nanosized crystallites, it was a more effective catalyst for the MPV reduction of 1,4-cyclohexanedione, bulky aldehydes and aromatic ketones. However, it is more susceptible to poisoning by water adsorption because of its hydrophilic nature. The easily scalable synthesis method allows a faster preparation of metal-substituted Lewis acid zeolites, although differences in textural and chemical properties should be taken into consideration when the material is applied as a catalyst.

1. Introduction

Zeolites with variable microporous topology, strong acidity and high stability are widely used as heterogeneous catalysts in the petrochemical industry and organic syntheses [1–5]. Lewis acid zeolites are of particular interest in fine chemical synthesis and biomass conversion [6–9]. In most cases, the Lewis acidity is caused by trivalent Al^{3+}. However, Lewis acid zeolites can also be obtained by the incorporation of tetravalent heteroatoms (e.g., Ti^{4+}, Zr^{4+} and Sn^{4+}) into the pure-silica zeolitic framework. A milestone in Lewis acid zeolites was the discovery of the titanosilicate TS-1, a titanium-containing zeolite with MFI topology [3]. It has been successfully commercialized in processes like propylene epoxidation, hydroxylation of phenol, and cyclohexanone ammoximation [10–14]. Tetravalent heteroatoms have also been incorporated into the framework of MWW and BEA type zeolites resulting in enhanced and sometimes unique catalytic activity [15–20]. For example, Sn-Beta or Zr-Beta zeolites are highly efficient for a wide range of organic reactions, including Baeyer-Villiger oxidation [21], intramolecular carbonyl-ene reaction [22–24], etherification [25], and Meerwein–Ponndorf–Verley (MPV) reduction [26–29]. More recently, transition metal-containing Beta zeolites caught the attention of researchers for biomass conversion owing to the superiority in activating carbonyl groups which are abundant in biomass-related molecules. These zeolites are used instead of enzymes to isomerize [30–35] or epimerize [36,37] sugars via intramolecular hydride shift in a MPVO redox cycle. Sn-Beta and Zr-Beta are also efficient catalysts for other biomass-related reactions, such as the conversion of sugar to lactic acid derivatives [38–40], furfural and levulinic acid to γ-valerolactone [41,42] and levoglucosenone to chiral γ-lactones [43].

Transition metal cations have larger radii than Si^{4+}. A fluoride medium instead of the conventional alkali medium is therefore necessary for the crystallization of these Lewis acid zeolites [17]. In a fluoride-mediated synthesis, the reaction takes place at neutral pH to avoid precipitation of the metal precursor as a metal oxide, which would make it unavailable for incorporation into the framework. However, due to the lower basicity, nucleation and crystal growth are delayed, resulting in long synthesis times (>20 days) and large crystals (>1 μm). Another drawback is the limited amount of substitution (Si/M > 75) [27].

* Corresponding author. Tel.: +65 65162839; fax: +65 67791691.
E-mail address: chmcgk@nus.edu.sg (G.-K. Chuah).
[1] Present address: Johnson Matthey (Shanghai) Catalyst Co., Ltd., 586 Dong Xing Road, Songjiang, Shanghai 201613, PR China.

http://dx.doi.org/10.1016/j.apcata.2015.01.001
0926-860X/

An alternative strategy to obtaining metal-substituted Beta zeolites is by post-synthesis of easily synthesized Al-Beta. Due to the excellent stability of the BEA framework, the aluminum can be removed via acid treatment whilst preserving the microporous topology. Dzwigaj and co-workers [44–48] found that by wet impregnation, a variety of transition-metal ions (e.g., V, Co, Ni, Fe, Cr) can be incorporated into the vacant tetrahedral sites of dealuminated Beta zeolite. In addition, chemical vapor deposition, solid state ion-exchange and grafting in isopropanol were attempted for the synthesis of Sn-Beta via post-synthetic routes [49–51]. These alternative syntheses make it possible to achieve a higher metal content in the framework while avoiding lengthy hydrothermal treatment. Furthermore, smaller crystals are obtained, which is beneficial for good mass transfer and diffusion.

These successful examples inspired us to develop zirconium-containing Beta zeolites with varying Si/Zr from 12.5 to 150 using the two-step post-synthesis method (Scheme 1). Zr-Beta with 8 wt% Zr (Si/Zr ~37) had been prepared by Hermans and collaborators using solid state impregnation with zirconium ethoxide [52]. Here, we apply the wet impregnation of dealuminated zeolite similar to that described by Dzwigaj et al. [44]. The procedure uses an aqueous metal salt, and the homogeneous solution ensures good reproducibility from batch to batch. The influence of the zirconium salt ($ZrOCl_2$ or $Zr(NO_3)_4$) for successful incorporation of zirconium into the zeolitic framework was investigated. The activity of the materials was compared with that of HF-synthesized zeolites, using the Meerwein–Ponndorf–Verley reduction of carbonyl compounds as test reaction. When fluoride anions are employed as mineralizing agent, zeolites formed are hydrophobic with low internal defect density, whereas zeolites synthesized using hydroxide anions are hydrophilic and contain vacancy defects in the framework. The extent to which these defects affect the performance of the zeolites is of interest. Furthermore, the ability to increase the density of metal active sites is exciting as it is expected to have a positive effect on the rate of reactions.

2. Experimental

2.1. Materials preparation

Commercial Beta zeolite (Zeolyst CP814E, Si/Al of 12.5) was dealuminated by treatment in nitric acid solution (12 M) at 80 °C for 20 h (10 mL g^{-1}). After filtration, the dealuminated powder (deAlβ) was thoroughly rinsed with water and dried overnight in an oven at 80 °C. Next, the dealuminated zeolite was suspended in water and the calculated amount of zirconium salt ($Zr(NO_3)_4$ or $ZrOCl_2{\cdot}8H_2O$) was added. The slurry was heated under stirring to remove the water, dried overnight at 80 °C in an oven and calcined at 600 °C for 8 h. The samples are denoted as Zrβ-NO_3-*x* or Zrβ-Cl-*x* depending on the zirconium precursor used and *x* = Si/Zr ratio of 12.5, 75 and 150.

The hydrothermal synthesis of Zr-Beta zeolite with Si/Zr ratio of 100 (Zrβ-F-100) in fluoride medium was carried out as previously reported [27]. Briefly, 10.42 g TEOS was mixed with 10.31 g tetraethyl-ammonium hydroxide (TEAOH, 40 wt% solution) and hydrolyzed under stirring. After 2 h, 1.55 g of an aqueous solution containing the required amount of $ZrOCl_2{\cdot}8H_2O$ was added dropwise. The mixture was stirred for another 7–8 h until the ethanol formed upon hydrolysis of TEOS was completely evaporated. Finally, 1.215 mL of HF (40% solution) and 0.105 g pure silica zeolite Beta seeds in 1 g of water were sequentially added. The crystallization was carried out in a Teflon-lined stainless steel autoclave at 140 °C for 20 days. The solid product obtained was filtered, washed with deionized water, dried at 100 °C and calcined at 580 °C for 10 h. For comparison of catalytic activity, mesoporous Zr-SBA-15 (with Si/Zr ratio of 10) and $Zr(OH)_4$ were prepared as reported elsewhere [42,53].

2.2. Characterization

Surface area and porosity of the samples were determined by nitrogen adsorption (Micromeritics Tristar 3000). Prior to each measurement, each sample was thoroughly degassed at 300 °C under a nitrogen flow for 4 h. The crystalline phase was determined by powder X-ray diffraction (Siemens D5005 equipped with Cu anode and variable slits). The diffractograms were recorded at a step size of 0.02° and a dwell time of 1 s. SEM images were obtained on a JEOL JSM-6701F field emission scanning electron microscope using 5 kV electron beam. Elemental composition of the catalysts was determined by inductively coupled plasma-atomic emission spectroscopy (ICP-AES) after dissolving the sample in a 1 mL of HF and diluting to 10 mL with deionized water. The diffuse reflectance spectra (DRS) were taken using a Shimadzu UV-2450 UV-Visible spectrophotometer. ^{29}Si MAS NMR spectra were measured on a Bruker DRX-400 widebore solid state spectrometer operating at a resonance frequency of 79.49 MHz with a spinning rate of 8 kHz, pulse length of 3 μs and a recycle delay of 20 s. 4 mm zirconia rotors were used and the ^{29}Si chemical shifts are reported relative to a TMS standard. Zr K edge (18.0 keV) XAFS data were collected at the BL01B1 station of the Japan Synchrotron Radiation Research Institute (JASRI). A Si(1 1 1) single crystal was used to obtain a monochromatic X-ray beam. The measurement was carried out in the quick mode. Ion chambers filled with N_2 (75%)/Ar (25%) and Ar (100%) were used to determine I_0 and I, respectively. The samples were pressed into self-supporting wafers. The data analysis was performed using the REX2000 Ver. 2.0.4 program (Rigaku). Fourier transformations of $k^3\chi(k)$ data were performed in the k range of 30–150 nm^{-1}. Infrared spectra of the samples were recorded in the range of 4000–400 cm^{-1} using a Bio-Rad Excalibur FT-IR spectrometer with a resolution of 1 cm^{-1}. Samples were pressed into self-supporting discs (10–20 mg) and pre-treated in an evacuated (<1 mbar) quartz cell with CaF_2 window at 450 °C for 6 h before measurements. To determine the Lewis and Brønsted acidity, the pyridine adsorption test was used. The samples were pretreated at 350 °C for 2 h before exposure to pyridine vapour (22 mbar) for 15 min, followed by re-evacuated at 100–300 °C for 1 h before measuring the IR spectra. The acidic nature of the samples was also quantified by temperature programmed desorption of NH_3. Samples were pretreated at 600 °C for 2 h in a flow of helium (50 mL min^{-1}). After cooling to 100 °C, NH_3 gas was introduced for 15 min. The sample was flushed with helium for another 2 h before heating at 10 °C min^{-1}. The desorption of NH_3 was monitored by a quadrupole mass spectrometer (Balzers Prisma 200). Thermogravimetric analyses to determine the water content were performed on a Dupont SDT 2960. The sample was first kept at 100 °C for 0.5 h to remove physically absorbed water, and then heated to 800 °C at 10 °C min^{-1}.

2.3. Catalytic tests

Prior to use, the samples were pre-activated at 500 °C for 1 h. Typically, for the MPV reduction, 1 mmol substrate and 5 mL of 2-propanol (65 mmol) were placed in a two-necked 25 mL round bottomed flask equipped with a septum port and a reflux condenser. The flask was heated to reflux temperature (82 °C) in an oil bath and the catalyst (100 mg) was added to the reaction mixture (0 min). The tested substrates include 1,4-cyclohexanedione (Sigma–Aldrich), acetophenone (Lancaster), 4-chloroacetophenone (Merck), benzylacetone (Sigma–Aldrich), cinnamaldehyde (Fluka), α-amyl cinnamaldehyde (Sigma–Aldrich) and citral (Fluka, *cis* + *trans*). For the MPV of 1,4-cyclohexandedione

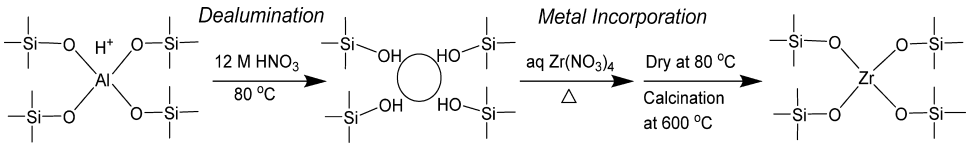

Scheme 1. Two-step post-synthetic strategy in the preparation of Zr-Beta.

and 4-*tert*-butylcyclohexanone, 2 and 5 mmol of the substrate, respectively, 5 mL of 2-propanol and 50 mg catalyst were used. Aliquots were taken at different times to follow the progress of reaction. The samples were analyzed by an Agilent HP 6890 gas chromatograph equipped with a HP-5 capillary column (250 μm × 0.25 μm × 30 m) and FID detector. The identity of the products was verified either by comparing the retention times with authentic samples or by GC–MS analyses. Mass balances were checked by calibration of the peaks with authentic samples and the error was within 3%.

3. Results and discussion

3.1. Physicochemical properties

In the first step, aluminum was removed from commercial Beta zeolite, β12.5 (Si/Al 12.5) by treatment with nitric acid to Si/Al > 1300. The surface area and microporosity were retained, indicating that the dealumination did not damage the crystallinity of the samples (Table 1). The samples were wet impregnated with zirconium nitrate or zirconyl chloride and calcined. Analysis by inductively coupled plasma-atomic emission spectroscopy (ICP-AES) showed that the zirconium content in the samples was close to the expected values (Table 1). Compared to the dealuminated zeolite, deAlβ, the surface area of the post-synthesized Zr-Beta samples was lower especially for those with high zirconium content (Si/Zr 12.5). Although the total pore volume of 0.94–1.28 $cm^3\ g^{-1}$ was relatively large, the micropore volume constituted only 0.16–0.17 $cm^3\ g^{-1}$. The bulk of the pore volume can be attributed to the interparticle space. From N_2 sorption measurements (Fig. S1), these pores were in the range of 20–50 nm, which agrees with the size of the particles observed in SEM (Fig. 1). The zeolite particles had a similar size as the dealuminated precursor zeolite, and no significant change occurred upon impregnation with the zirconium salts. In contrast, the Zr-Beta prepared by hydrothermal synthesis using HF, Zrβ-F-100, had a total pore volume of only 0.27 $cm^3\ g^{-1}$ with the bulk of it being due to micropores. The zeolite particles formed are much larger, in the order of 1–2 μm. This is due to the long crystallization time required for the fluoride-mediated synthesis.

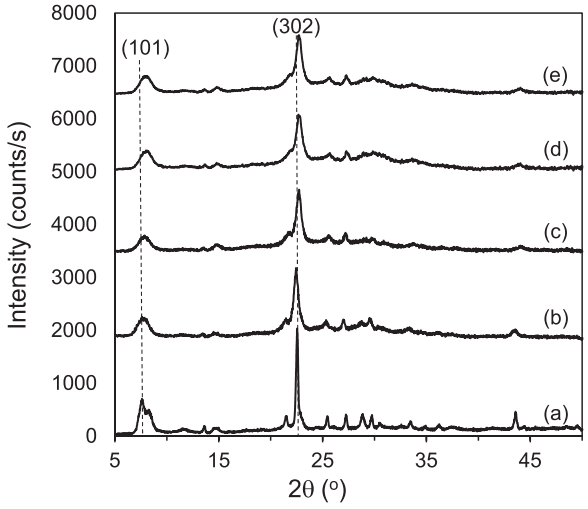

Fig. 2. X-ray diffractograms of (a) Zrβ-F-100, (b) β-12.5, (c) deAlβ, (d) Zrβ-NO_3-12.5 and (e) Zrβ-Cl-12.5.

The X-ray diffractogram of Zrβ-F-100 (Fig. 2) shows sharp diffraction peaks of well-crystallized zeolite Beta, in agreement with the large crystallites observed in the electron micrographs. Zeolite beta comprises two closely related and highly intergrown polymorphs, and the crystals have a high planar stacking fault density [54]. As a result, the X-ray diffractogram contains narrow as well as broad reflections. The shoulder at the higher angle side of the ~8° peak indicates a slight preference for one of the two polymorphs. In comparison, the commercial Beta zeolite gave broader peaks of lower intensity, indicative of smaller crystallites. The crystallite size remained essentially unchanged after dealumination and subsequent impregnation with $Zr(NO_3)_4$. However, the position of the (3 0 2) peak at $2\theta \sim 22.6°$ shifted slightly in response to the changes of composition. Dealumination of β-12.5 resulted in a decrease in the interplanar distance, *d*, for the (3 0 2) planes from 3.950 Å to 3.906 Å, indicating a contraction of the BEA matrix. Following the incorporation of zirconium into the zeolite framework, the $d_{(302)}$-spacing in Zrβ-NO_3-12.5 increased again to 3.919 Å. Even

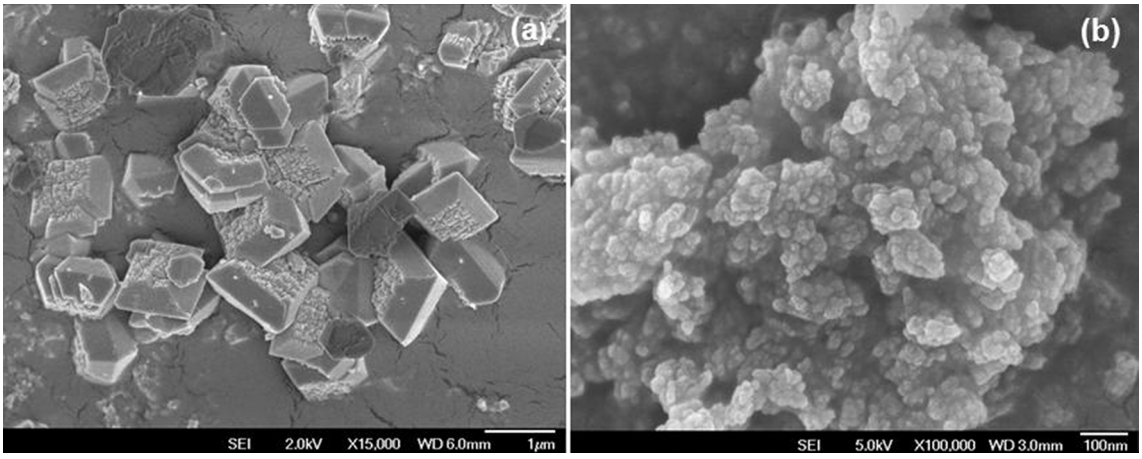

Fig. 1. SEM images of (a) Zrβ-F-100 and (b) Zrβ-NO_3-12.5.

Table 1
Physicochemical properties of the samples.

Samples	Si/Al[a]	Si/Zr[a]	S_{BET} ($m^2\ g^{-1}$)	V_{micro} ($cm^3\ g^{-1}$)	V_{total} ($cm^3\ g^{-1}$)
β-12.5	12	–	537	0.17	1.21
deAlβ	>1300	–	521	0.17	1.14
Zrβ-Cl-12.5	>1300	12	464	0.17	0.94
Zrβ-NO_3-12.5	>1300	12	475	0.16	0.91
Zrβ-NO_3-75	>1300	73	495	0.16	1.23
Zrβ-NO_3-150	>1300	157	502	0.17	1.28
Zrβ-F-100	–	107	474	0.20	0.27

[a] Determined by ICP-AES.

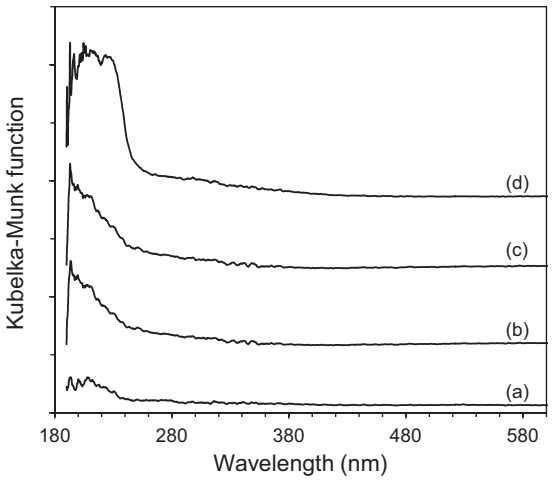

Fig. 3. UV/vis diffuse reflectance spectra of (a) deAlβ, (b) Zrβ-NO_3-12.5, (c) Zrβ-Cl-12.5 and (d) ZrO_2.

with the highest zirconium content (Si/Zr 12.5), no diffraction lines corresponding to bulk ZrO_2 particles were observed. The absence of bulk ZrO_2 was confirmed by the lack of a sharp absorption edge at ~240 nm in the UV–vis diffuse reflectance spectrum (DRS) (Fig. 3).

The existence of very small ZrO_2 crystallites is difficult to detect by XRD and DRS. Therefore, the dispersion of zirconium was further characterized by extended X-ray absorption fine structure (EXAFS). The EXAFS spectrum of Zrβ-Cl-12.5 showed a rapid oscillation on the Zr K edge. The Fourier transform of the EXAFS data shows an obvious peak at around 3.4 Å (Fig. 4), which corresponds to the Zr—O—Zr bond distance [55]. In contrast, for Zrβ-NO_3-12.5, the Zr—O—Zr oscillation was smaller, indicating less ZrO_2 aggregation in samples synthesized using $Zr(NO_3)_4$ as precursor than with $ZrOCl_2{\cdot}H_2O$. Furthermore, the peak at 3.0 Å in the Fourier transform spectrum of Zrβ-NO_3-12.5 has a higher amplitude than in Zrβ-Cl-12.5. This peak is assigned to the Zr—O—Si bond. Hence, the choice of the zirconium source, $Zr(NO_3)_4$ or $ZrOCl_2$, used for wet impregnation appears to affect the dispersion of zirconium. For Zrβ-F-100, synthesized under fluoride-mediated hydrothermal conditions, the Zr—O—Zr peak at 3.4 Å is very small, pointing to the highest dispersion of zirconium amongst the samples. This is not unexpected because the zirconium content in this sample is much lower than in the post-synthesized samples.

The incorporation of zirconium into the framework was also followed by FT-IR (Fig. 5). The commercial Al-Beta zeolite exhibits a sharp band at 3745 cm^{-1} and a weak band at ca. 3780 m^{-1}, indicative of terminal Si-OH and Al-OH groups, respectively [51]. After dealumination, the band at 3780 cm^{-1} disappeared, indicating the absence of Al-OH groups. Instead, the opening of silanol nests and the creation of vacant tetrahedral T-sites resulted in a broad band at around 3500 cm^{-1}. Following the zirconium incorporation, the broad band disappeared, consistent with the consumption of silanol nests.

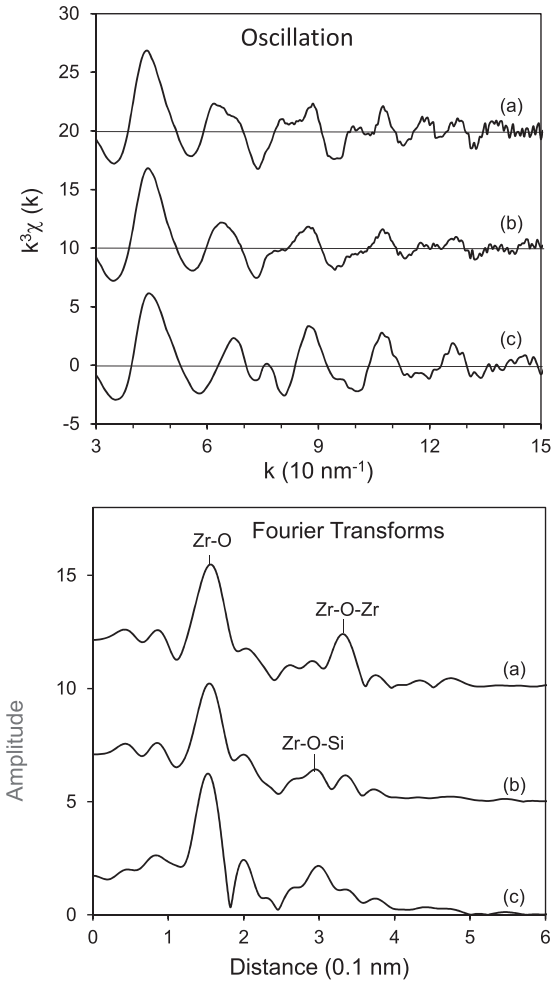

Fig. 4. EXAFS data of Zr K edge and Fourier transforms for (a) Zrβ-Cl-12.5, (b) Zrβ-NO_3-12.5 and (c) Zrβ-F-100.

^{29}Si MAS NMR was used to study the change in the chemical environment before and after zirconium incorporation (Fig. 6). The spectrum of the dealuminated sample shows three peaks at ca. −104, −112 and −114 ppm. The broad peak at −104 ppm corresponds to Si atoms in a Q^3 ($Si(OH)(OSi)_3$) environment, while the latter two peaks are due to $Si(OSi)_4$ (Q^4) at different crystallographic sites [56,57]. The Q^3 environment is derived from structural defects of connectivity (Si-O- or Si-OH groups). The incorporation of zirconium into the vacant T-atom sites consumes the terminal Si-OH groups, leading to a reduction in the intensity of the Q^3 peak at ca. −102 ppm. Furthermore, the Zrβ-NO_3-12.5 sample has three broad Q^4 resonances at ca. −112, −113 and −116 ppm. These overlapping resonances are caused by $Si(OSi)_4$ and $Si(OSi)_3OZr$ at different crystallographic sites, similar to that of Zr-Beta prepared in the fluoride medium [27].

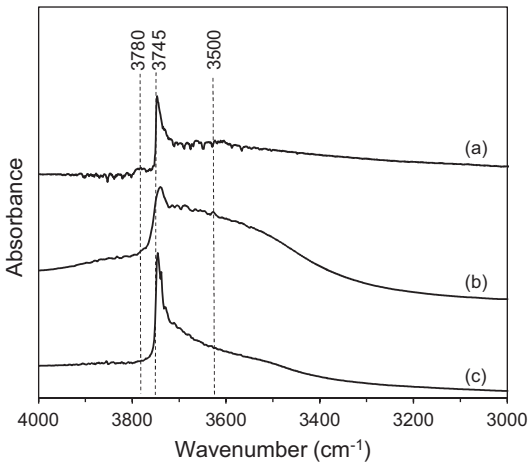

Fig. 5. FT-IR spectra of (a) β-12.5, (b) deAlβ and (c) Zrβ-NO_3-12.5 samples.

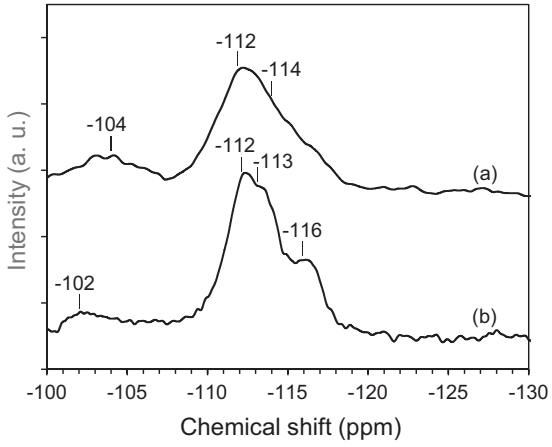

Fig. 6. Solid state ^{29}Si MAS NMR of (a) deAlβ and (b) Zrβ-NO_3-12.5.

3.2. Acidity measurements

The acidic properties were studied using NH_3-TPD (Fig. 7) and pyridine FTIR (Fig. 8). The desorption of NH_3 from Zrβ-F-100 occurred between 220 and 380 °C with a maximum at ~300 °C. From the amount of desorbed NH_3, the density of acid sites was calculated to be 45 μmol g^{-1}. Desorption of NH_3 from the post-synthesized Zr-Beta zeolites (Si/Zr 12.5–150) occurred over a wider

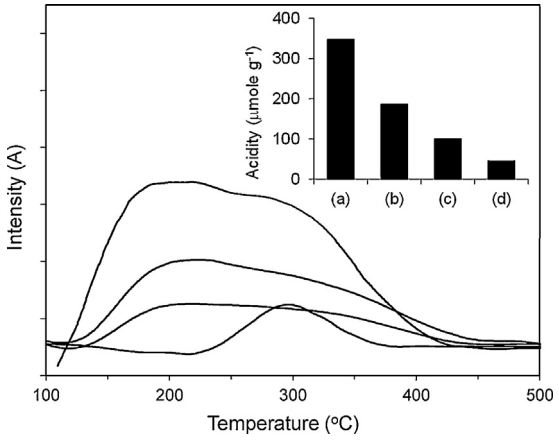

Fig. 7. NH_3-TPD profiles of (a) Zrβ-NO_3-12.5, (b) Zrβ-NO_3-75, (c) Zrβ-NO_3-150 and (d) Zrβ-F-100.

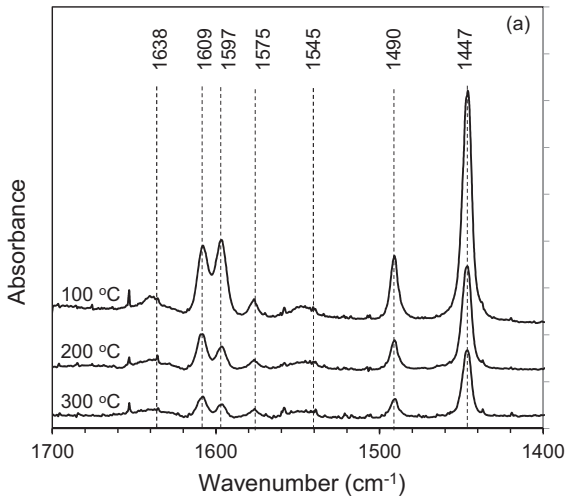

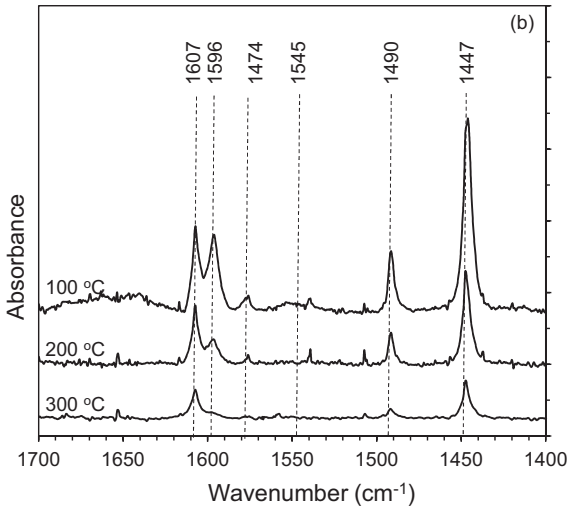

Fig. 8. Infrared spectra of (a) Zrβ-NO_3-12.5 and (b) Zrβ-F-100 after pyridine adsorption and subsequent desorption at the indicated temperatures.

temperature range, from 130 to 480 °C, showing that these materials contained sites with low as well as high acid strength. Although physically adsorbed NH_3 might contribute to desorption below 200 °C, this was minimized by flushing the sample with helium for 2 h prior to the measurements. Silanol nests that are not taken up by zirconium or partially hydrolyzed framework zirconium could add to the wide range of acidity in the post-synthesized samples. The acidity of Sn-Beta is well studied, and the weak Brønsted acidity has been attributed to residual unoccupied silanol nests [58]. The Sn exists as nonhydrolyzed Sn(-O-Si-)$_4$ or partially hydrolyzed (-Si-O-)$_3$Sn-OH, and the former was shown to be a weaker Lewis acid than the latter [58,59]. The density of acid sites in the post-synthesis modified material was higher than for the HF-synthesized zeolite (Fig. 7, inset). The concentration of acid sites increased with the amount of Zr incorporated, from 100 μmol g^{-1} for a sample with Si/Zr = 150 to 347 μmol g^{-1} for that with Si/Zr = 12.5. Even at a Si/Zr of 150, the post-synthesized Zrβ-NO_3-150 contained about twice as many acid sites as Zrβ-F-100. The pyridine IR spectra of the post-synthesized Zrβ-NO_3-12.5 sample show absorption bands indicative of Lewis and Brønsted acidity even after heating to 300 °C (Fig. 8). Pyridine coordinatively bound to Lewis acid sites have vibrational modes at ~1447–1460, 1488–1503, 1580 and 1600–1633 cm^{-1} [60,61]. The adsorption of pyridine at Brønsted acid site leads to the formation of the pyridinium ion which has vibrational modes at 1485–1500, 1530–1550 and 1630–1640 cm^{-1}.

Table 2
Catalytic activity for MPV reduction of 4-*tert*-butylcyclohexanone.

Entry	Catalyst	Conv. (%)[a]	*cis* Sel. (%)	Rate (mmol g^{-1} h^{-1})[b]	TOF_{Zr} (h^{-1})[b]
1	deAlβ	0	–	–	–
2	Zrβ-F-100	98[c]	>99	87.2	522
3	Zrβ-Cl-12.5	31	>99	23.5	20.2
4	Zrβ-NO_3-12.5	94	>99	62.6	49.6
5	Zrβ-NO_3-75	97	>99	62.0	283
6	Zrβ-NO_3-150	71	>99	39.2	353
7	$Zr(OH)_4$	62[d]	18	–	–
8	ZrSBA-15	24	17	–	–
9	Zrβ-NO_3-12.5[e]	0	–	–	–
10	Zrβ-NO_3-12.5[f]	83	>99	–	–

[a] Reaction conditions: 5 mmol 4-*tert*-butylcyclohexanone, 5 mL 2-propanol, 50 mg catalyst, 82 °C, 6 h.
[b] Based on the conversion of initial 30 min.
[c] After 2 h.
[d] After 20 h.
[e] Sample hydrated in air.
[f] Sample re-activated by calcination at 500 °C for 1 h.

In particular, the band at 1530–1550 cm^{-1} can be unambiguously assigned to Brønsted acidity as it does not overlap with any bands arising from coordinatively bonded pyridine. For Zrβ-F-100, the 1530–1550 cm^{-1} band was very weak, and after heating to 200 °C or above, only the absorption bands due to coordinatively bonded pyridine were observed. This indicates that the fluoride-synthesized zeolite contained predominantly Lewis acid sites. For comparison, the pyridine IR spectra of dealuminated zeolite, deAlβ, show absorption bands centered at 1445 and 1595 cm^{-1} together with a very weak absorption in the 1485–1500 cm^{-1} region (Fig. S3). These bands are indicative of pyridine hydrogen-bonded to surface hydroxyl groups and/or bonded to very weak Lewis acid sites. As deAlβ is highly siliceous, it lacks strong Lewis acidity.

3.3. MPV reduction of 4-tert-butylcyclohexanone

To evaluate the catalytic performance of the post-synthesized Zr-Beta samples, their activity for the Meerwein–Ponndorf–Verley (MPV) reduction of 4-*tert*-butylcyclohexanone was investigated. We have previously reported that Zr-Beta synthesized using HF under hydrothermal conditions showed excellent activity and stereoselectivity for this reaction, with *cis*-4-*tert*-butylcyclohexanol as the only detectable product [27]. Indeed, an initial turnover frequency based on zirconium sites (TOF_{Zr}) of 522 h^{-1} was obtained over Zrβ-F-100 (Table 2). Zirconium ions in the zeolitic framework are the active sites because dealuminated pure silica Beta zeolite showed no activity at all. The TOF_{Zr} was lower for post-synthesized Zr-Beta than for Zr-Beta synthesized hydrothermally using HF. For Zr-Beta prepared using $ZrOCl_2 \cdot 8H_2O$, the initial TOF_{Zr} was only 20.2 h^{-1}. This zeolite had a much higher zirconium content than the fluoride-synthesized sample, Si/Zr 12.5 vs 100 (Table 2, entry 3). The lower activity per site may be due to a lower dispersion of the zirconium species, as deduced from the EXAFS results. Post-synthesis with $Zr(NO_3)_4$ as zirconium source resulted in more active samples, and conversions of 71 to 97% were obtained after 6 h. The rate of reaction decreased with the reduction of zirconium content. However, the TOF_{Zr} was 353 h^{-1} in Zrβ-NO_3-150 and only 49.6 h^{-1} for Zrβ-NO_3-12.5. This decrease in TOF shows that a higher Zr loading leads to a less effective use of each zirconium site. A similar trend had been reported for Sn-Beta where a higher Sn-loading did not help to boost the rate of sugar isomerization [51].

Irrespective of the mode of synthesis, all the zeolites showed excellent stereoselectivity (>99%) toward *cis*-4-*tert*-butylcyclohexanol. This has been attributed to a pore size constraint effect on the transition state of the reaction. The MPV

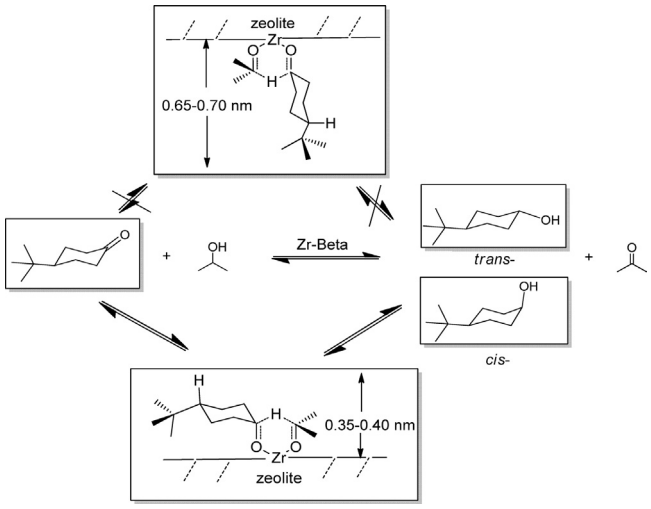

Scheme 2. Illustration of the transition states leading to *cis*- and *trans*-4-*tert*-butylcyclohexanol over Zr-Beta.

reaction is proposed to occur via a six-membered transition state formed by the chemisorption of the *sec*-alcohol and the ketone at the Lewis acid site (Scheme 2). Hydrogen from the C—H bond of the alcohol is transferred to the carbonyl carbon of the acceptor. When the active Lewis acid site is located inside the zeolitic framework, the transition state leading to the *cis*-alcohol is preferred as it is more aligned with the BEA channel than that for the *trans*-alcohol [27,62]. The size of the transition state to the *trans*-alcohol with an axially oriented form is around 0.65–0.70 nm, which is difficult to accommodate in the BEA channels (ca. 0.66 nm × 0.67 nm). However, mesoporous materials such as $Zr(OH)_4$ or Zr-SBA-15, where pore constraints are not an issue, give the *trans*-alcohol as the main product (Table 2, entries 7 and 8). Hence, the high stereoselectivity to *cis*-4-*tert*-butylcyclohexanol indicates that the zirconium in the post synthesized Zr-Beta has to be well dispersed within the zeolite framework. The heterogeneous nature of the catalyst was confirmed by removal of the catalyst after 2 h when the conversion had reached 58% (Fig. S4). No increase in conversion was observed in the residual solution after removal of the catalyst.

3.4. Scope of MPV reduction

We conducted the MPV reduction of other substrates to compare the performance of the post-synthesized and hydrothermally synthesized Zr-Beta zeolites. The MPV reduction of 1,4-cyclohexanedione gives initially 4-hydroxycyclohexanone, which can be further reduced to 1,4-cyclohexanediol. The diol is potentially useful as a penetrant in dermatological formulations [63]. Over Zrβ-F-100 as catalyst, the conversion of 1,4-cyclohexanedione required 18 h to reach >97% (Fig. 9a). The yield of 4-hydroxycyclohexanone reached a maximum of 56% after 8 h. However, the subsequent reduction of 4-hydroxycyclohexanone to 1,4-cyclohexanediol was rate limiting with the rate being 13.5 times lower than the first step. Hence, even after 18 h, the reaction mixture still contained about 30% 4-hydroxycyclohexanone. The reduction of 4-hydroxycyclohexanone to 1,4-cyclohexanediol was faster over the post-synthesized Zrβ-NO_3-100 and after 18 h, a higher yield of 1,4-cyclohexanediol was obtained. As both Zrβ-F-100 and Zrβ-NO_3-100 have the same zirconium content, the higher reaction rate may be due to the smaller particle size of the latter which would facilitate diffusion to active sites within the pore channels. Furthermore, the concentration of 1,4-cyclohexanedione and its intermediate in the pore channels depends on the hydrophobic/hydrophilic balance at the surface of the two catalysts. In a more

hydrophilic environment, the concentration of the polar intermediate, 4-hydroxycyclohexanone, will be higher, enhancing its rate of reduction to the diol.

With Zrβ-NO_3-12.5, where the zirconium content is higher, the conversion of 1,4-cyclohexanedione reached >97% after only 6 h (Fig. 9b). The maximum yield of 4-hydroxycyclohexanone, 46%, was obtained after only 2 h, and complete reduction to 1,4-cyclohexanediol occurred after 18 h. Although each site may be less active than in Zrβ-F-100, the much greater number of sites increases the probability of reaction, thus giving a higher overall reaction rate.

Next, we investigated the MPV reduction of aromatic ketones which are harder to reduce than aliphatic or cyclic ketones due to steric hindrance at the C=O posed by the rigid benzene ring. In such a case, a higher density of active sites in the post-synthesized Zr-Beta might be useful to increase the chances of encounters. The reduction of acetophenone and 4-chloro-acetophenone using Zrβ-F-100 requires a longer time than 4-*tert*-butylcyclohexanone even with a higher catalyst loading (Table 3, entries 1 & 2). After 18 h, the conversion of acetophenone and 4-chloro-acetophenone was 61 and 65%, respectively. In comparison, with Zrβ-NO_3-12.5 as the catalyst, the initial rates were at least two times higher than for Zrβ-F-100 and after 18 h, the conversion of acetophenone and 4-chloro-acetophenone was 86 and 98%, respectively. In benzyl acetone, the aromatic ring is at the β-position and the molecule reacts faster than the acetophenones. Over the post-synthesized Zrβ-NO_3-12.5, full conversion was reached after 6 h compared to only 56% for ZrβF-100 (Table 3, entry 3). These results show that a higher Zr density is helpful in increasing the rate of reaction for these substrates. Furthermore, the smaller particle size of the post-synthesized sample allows an easier access to the Zr sites located in the pore channels.

We have previously found that Zrβ-F-100 showed very good activity and chemoselectivity in the reduction of cinnamaldehyde to cinnamyl alcohol [29]. However, this catalyst could not reduce the more bulky amyl cinnamaldehyde as effectively, giving only 33% conversion after 24 h. The use of Zrβ-NO_3-12.5 is clearly advantageous for this substrate as the conversion was almost doubled, 62%, after a similar time. Similarly, a higher conversion of citral was obtained over Zrβ-NO_3-12.5 than with Zrβ-F-100 (Table 3, entry 6). However, the selectivity to geraniol and nerol was reduced due to dehydration and was slightly lower for the more acidic Zrβ-NO_3-12.5. For these bulky substrates, post-synthesized zeolites are efficient catalysts because their small particle size, 20–50 nm, translates into shorter diffusion paths for the molecule to reach the active sites in the pore channels.

3.5. Hydrophilicity of post-synthesized Zr-Beta

The above results show that the post-synthesized Zrβ-NO_3-12.5 with a higher zirconium content is more active than the hydrothermally-prepared Zrβ-F-100 for the MPV reduction of 1,4-cyclohexanedione, aromatic ketones and bulky aldehydes. However, we observed that the post-synthesized sample, when left in the open for some time, became totally inactive for the MPV reduction of 4-*tert*-butylcyclohexanone (Table 2, entry 9). This is in contrast to the robust and easy-to-handle nature of the HF-synthesized Zr-Beta. For the post-synthesized zeolite, recalcination at 500 °C for 1 h was necessary in order to fully regenerate its activity (Table 2, entry 10). It is known that samples prepared by post-synthesis and hydrothermal synthesis differ in their surface hydrophobicity [64,65]. The post-synthesized zeolites have a higher density of silanol groups than zeolites synthesized hydrothermally in fluoride. The water adsorption capacity was examined by thermogravimetric analysis after drying the samples at 100 °C for 30 min. The Zrβ-F-100 showed a weight loss of only 2.2% from 100 to 800 °C while Zrβ-NO_3-12.5 had a much higher weight loss of 7.6% (Table 4 and Fig. S5). The weight loss is due to the removal of adsorbed water at low temperatures (<200 °C) and water from surface OH-groups at high temperatures. These

Table 3
MPV reduction of various substrates.

Entry	Substrate	Catalyst	Time (h)	Yield (%)	Rate (mmol $g^{-1}h^{-1}$)[a]	TOF_{Zr} (h^{-1})[a]
1	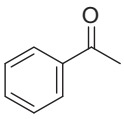	Zrβ-F-100	18	61	0.23	1.3
		Zrβ-NO_3-12.5	18	86	0.52	0.5
2	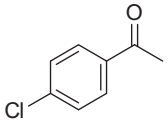	Zrβ-F-100	18	65	0.58	3.4
		Zrβ-NO_3-12.5	18	98	1.35	1.2
3	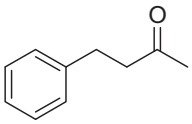	Zrβ-F-100	6	56	1.64	9.8
		Zrβ-NO_3-12.5	6	100	3.40	3.0
4	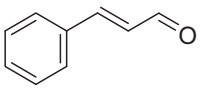	Zrβ-F-100	3	98	4.16	24.9
		Zrβ-NO_3-12.5	3	88	3.92	3.4
5	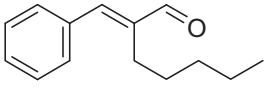	Zrβ-F-100	24	33	0.15	0.9
		Zrβ-NO_3-12.5	24	62	0.27	0.2
6	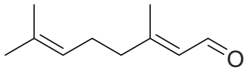	Zrβ-F-100	4	67	2.25	13.4
		Zrβ-NO_3-12.5	4	80	2.94	2.6

Reaction conditions: 1 mmol substrate, 5 mL 2-propanol, 100 mg catalyst, 82 °C.
[a] Based on the conversion over the initial 30 min or 2 h (entries 1, 2 and 5).

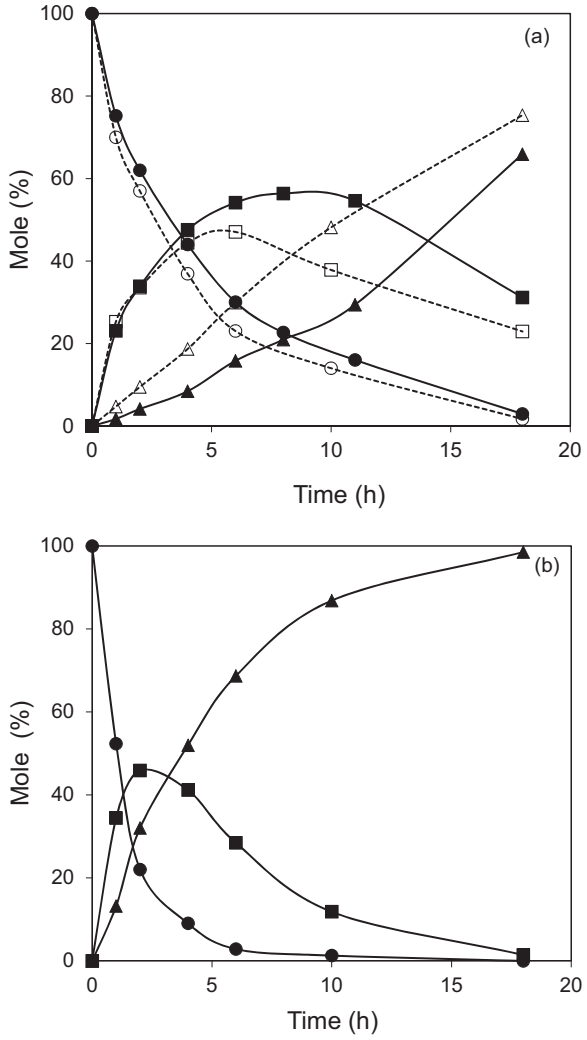

Fig. 9. MPV reduction of 1,4-cyclohexanedione over (a) Zrβ-F-100 and Zrβ-NO_3-100 (dashed lines) and (b) Zrβ-NO_3-12.5. (•, ○) 1,4-cyclohexanedione; (■, □) 4-hydroxycyclohexanone; (▲,△) 1,4-cyclohexanediol.

Table 4
Weight loss of Zrβ-NO_3-12.5 and Zrβ-F-100.

Sample	Weight loss (%)	
	I (100–200 °C)	II (200–800 °C)
Zrβ-NO_3-12.5	4.6	2.8
Zrβ-F-100	1.1	1.1

results show that the post-synthesized zeolite easily binds molecular water, while the Beta zeolite synthesized in fluoride media is more water-resistant. Being more susceptible to water poisoning, it is necessary to thoroughly dry the post-synthesized zeolites before use. Furthermore, their catalytic performance will be affected in reactions where water is produced [64,66] in contrast to the water tolerance shown by the Zr-Beta hydrothermally synthesized in a fluoride medium [27].

4. Conclusion

Zirconium can be incorporated into the framework of dealuminated Beta zeolite to form Lewis acid catalysts. The two-step post-synthesis method shortens the long synthesis time of >20 days to only 3 days, and avoids the use of HF required in the conventional synthesis of Zr-Beta. Characterization by FT-IR, ^{29}Si MAS NMR, XRD and DRS indicates that the zirconium species are highly dispersed within the framework, but EXAFS revealed the existence of some Zr—O—Zr bonds in Zr-Beta with Si/Zr loading of 12.5. The post-synthesized samples have a higher density of acid sites than Zr-Beta synthesized hydrothermally in fluoride medium. In the MPV reduction of 4-*tert*-butylcyclohexanone, the post-synthesized Zr-Beta catalysts exhibit a similarly high stereoselectivity toward *cis*-4-*tert*-butylcyclohexanol, >99%, which supports the assumption that the zirconium sites are located within the zeolitic framework. Compared to Zrβ-F-100, the post-synthesized Zrβ-NO_3-12.5 had higher activity for the MPV reduction of 1,4-cyclohexanedione, aromatic ketones and bulky aldehydes, which can be attributed to the higher zirconium substitution level and the smaller particle size. TGA measurements revealed a higher adsorption of water at the surface of the post-synthesized Zr-Beta than on the hydrophobic HF-synthesized zeolite. Hence, it is necessary to activate the samples prior to catalytic testing.

Acknowledgement

This work is financially supported by Ministry of Education, Singapore, ARC Tier 1 grants R-143-000-476-112 and R-143-000-550-112.

Appendix A. Supplementary data

Supplementary data associated with this article can be found, in the online version, at http://dx.doi.org/10.1016/j.apcata.2015.01.001.

References

[1] A. Corma, Chem. Rev. 97 (1997) 2373–2420.
[2] M.E. Davis, Nature 417 (2002) 813–821.
[3] C.S. Cundy, P.A. Cox, Chem. Rev. 103 (2003) 663–702.
[4] R. Xu, W. Pang, J. Yu, Q. Huo, J. Chen, Chemistry of Zeolites and Related Porous Materials: Synthesis and Structure, John Wiley & Sons, Singapore, 2009.
[5] H. van Bekkum, H.W. Kouwenhoven, Zeolite Manual for the Organic Chemist, Mijnbestseller, Netherlands, 2012.
[6] A. Corma, H. Garcia, Chem. Rev. 103 (2003) 4307–4366.
[7] E. Taarning, C.M. Osmundsen, X.B. Yang, B. Voss, S.I. Andersen, C.H. Christensen, Energy Environ. Sci. 4 (2011) 793–804.
[8] M. Dusselier, P. van Wouwe, A. Dewaele, E. Makshina, B.F. Sels, Energy Environ. Sci. 6 (2013) 1415–1442.
[9] M. Moliner, Dalton Trans. 43 (2014) 4197–4208.
[10] M. Taramasso, G. Perego, B. Notari, US Patent 4,410,501, 1983.
[11] M.G. Clerici, P. Ingallina, US Patent 5,221,795, 1993.
[12] R.A. Sheldon, M. Wallau, I.W. Arends, U. Schuchardt, Acc. Chem. Res. 31 (1998) 485–493.
[13] G. Paparatto, A. Forlin, P. Tegon, EP Patent 1,072,599, 2004.
[14] F. Cavani, J.H. Teles, ChemSusChem 2 (2009) 508–534.
[15] A. Corma, M. Camblor, P. Esteve, A. Martinez, J. PerezPariente, J. Catal. 145 (1994) 151–158.
[16] T. Tatsumi, N. Jappar, J. Phys. Chem. B 102 (1998) 7126–7131.
[17] S.V. Valencia, A.C. Canos, US Patent 5,968,473A, 1999.
[18] P. Wu, T. Tatsumi, T. Komatsu, T. Yashima, Chem. Lett. 29 (2000) 774–775.
[19] A. Corma, L.T. Nemeth, M. Renz, S. Valencia, Nature 412 (2001) 423–425.
[20] Y. Zhu, G. Chuah, S. Jaenicke, Chem. Commun. (2003) 2734–2735.
[21] M. Renz, T. Blasco, A. Corma, V. Fornés, R. Jensen, L. Nemeth, Chem. Eur. J. 8 (2002) 4708–4717.
[22] A. Corma, M. Renz, Chem. Commun. (2004) 550–551.
[23] Y. Zhu, Y.T. Nie, S. Jaenicke, G.-K. Chuah, J. Catal. 229 (2005) 404–413.
[24] Y.T. Nie, S. Jaenicke, G.-K. Chuah, Chem. Eur. J. 15 (2009) 1991–1999.
[25] A. Corma, M. Renz, Angew. Chem. Int. Ed. 46 (2007) 298–300;
A. Corma, M. Renz, Angew. Chem. 119 (2007) 302–304.
[26] A. Corma, M.E. Domine, L. Nemeth, S. Valencia, J. Am. Chem. Soc. 124 (2002) 3194–3195.
[27] Y. Zhu, G. Chuah, S. Jaenicke, J. Catal. 227 (2004) 1–10.
[28] M. Boronat, A. Corma, M. Renz, J. Phys. Chem. B 110 (2006) 21168–21174.
[29] Y. Zhu, G.-K. Chuah, S. Jaenicke, J. Catal. 241 (2006) 25–33.
[30] Y. Román-Leshkov, M. Moliner, J.A. Labinger, M.E. Davis, Angew. Chem. Int. Ed. 49 (2010) 8954–8957;
Y. Román-Leshkov, M. Moliner, J.A. Labinger, M.E. Davis, Angew. Chem. 122 (2010) 9138–9141.

[31] M. Moliner, Y. Román-Leshkov, M.E. Davis, Proc. Natl. Acad. Sci. U. S. A. 107 (2010) 6164–6168.
[32] C.M. Lew, N. Rajabbeigi, M. Tsapatsis, Ind. Eng. Chem. Res. 51 (2012) 5364–5366.
[33] R. Bermejo-Deval, R.S. Assary, E. Nikolla, M. Moliner, Y. Román-Leshkov, S.-J. Hwang, A. Palsdottir, D. Silverman, R.F. Lobo, L.A. Curtiss, Proc. Natl. Acad. Sci. U. S. A. 109 (2012) 9727–9732.
[34] S. Saravanamurugan, M. Paniagua, J.A. Melero, A. Riisager, J. Am. Chem. Soc. 135 (2013) 5246–5249.
[35] R. Gounder, M.E. Davis, ACS Catal. 3 (2013) 1469–1476.
[36] W.R. Gunther, Y. Wang, Y. Ji, V.K. Michaelis, S.T. Hunt, R.G. Griffin, Y. Román-Leshkov, Nat. Commun. 3 (2012) 1109.
[37] R. Bermejo-Deval, R. Gounder, M.E. Davis, ACS Catal. 2 (2012) 2705–2713.
[38] E. Taarning, S. Saravanamurugan, M.S. Holm, J. Xiong, R.M. West, C.H. Christensen, ChemSusChem 2 (2009) 625–627.
[39] M.S. Holm, S. Saravanamurugan, E. Taarning, Science 328 (2010) 602–605.
[40] M.S. Holm, Y.J. Pagán-Torres, S. Saravanamurugan, A. Riisager, J.A. Dumesic, E. Taarning, Green Chem. 14 (2012) 702–706.
[41] L. Bui, H. Luo, W.R. Gunther, Y. Román-Leshkov, Angew. Chem. Int. Ed. 52 (2013) 8022–8025;
L. Bui, H. Luo, W.R. Gunther, Y. Román-Leshkov, Angew. Chem. 125 (2013) 8180–8183.
[42] J. Wang, S. Jaenicke, G.-K. Chuah, RSC Adv. 4 (2014) 13481–13489.
[43] A. Corma, C. Paris, M. Moliner, Green Chem. 15 (2013) 2101–2109.
[44] S. Dzwigaj, M. Peltre, P. Massiani, A. Davidson, M. Che, T. Sen, S. Sivasanker, Chem. Commun. (1998) 87–88.
[45] S. Dzwigaj, M. Che, J. Phys. Chem. B 110 (2006) 12490–12493.
[46] S. Dzwigaj, T. Shishido, J. Phys. Chem. C 112 (2008) 5803–5809.
[47] S. Dzwigaj, J.-P. Nogier, M. Che, M. Saito, T. Hosokawa, E. Thouverez, M. Matsuoka, M. Anpo, Catal. Commun. 19 (2012) 17–20.
[48] A. Śrębowata, R. Baran, D. Łomot, D. Lisovytskiy, T. Onfroy, S. Dzwigaj, Appl. Catal. B 147 (2014) 208–220.
[49] P. Li, G. Liu, H. Wu, Y. Liu, J.-G. Jiang, P. Wu, J. Phys. Chem. C 115 (2011) 3663–3670.
[50] C. Hammond, S. Conrad, I. Hermans, Angew. Chem. Int. Ed. 51 (2012) 11736–11739;
C. Hammond, S. Conrad, I. Hermans, Angew. Chem. 124 (2012) 11906–11909.
[51] J. Dijkmans, D. Gabriëls, M. Dusselier, F. de Clippel, P. Vanelderen, K. Houthoofd, A. Malfliet, Y. Pontikes, B.F. Sels, Green Chem. 15 (2013) 2777–2785.
[52] P. Wolf, C. Hammond, S. Conrad, I. Hermans, Dalton Trans. 43 (2014) 4514–4519.
[53] D.M. Do, S. Jaenicke, G.-K. Chuah, Catal. Sci. Technol. 2 (2012) 1417–1424.
[54] J.M. Newsam, M.M.J. Treacy, W.T. Koetser, C.B. de Gruyter, Proc. R. Soc. Lond. A 420 (1988) 375.
[55] K. Okumura, Y. Iwasawa, J. Catal. 164 (1996) 440–448.
[56] E.B. Lami, F. Fajula, D. Anglerot, T. des Courieres, Microporous Mater. 1 (1993) 237–245.
[57] M. Trejda, M. Ziolek, Y. Millot, K. Chalupka, M. Che, S. Dzwigaj, J. Catal. 281 (2011) 169–176.
[58] M. Boronat, P. Concepción, A. Corma, M. Renz, S. Valencia, J. Catal. 234 (2005) 111–118.
[59] R. Bermejo-Deval, M. Orazov, R. Gounder, S.-J. Hwang, M.E. Davis, ACS Catal. 4 (2014) 2288–2297.
[60] E.P. Parry, J. Catal. 2 (1963) 371–379.
[61] J.A. Boscoboinik, X. Yu, E. Emmez, B. Yang, S. Shaikhutdinvo, F.D. Fischer, J. Sauer, H.-J. Freund, J. Phys. Chem. C 117 (2013) 13547–13556.
[62] E. Creyghton, S. Ganeshie, R. Downing, H. van Bekkum, J. Mol. Catal. A 115 (1997) 457–472.
[63] N. Li, W. Jia, Y. Zhang, F. Tan, J. Zhang, Int. J. Pharm. 415 (2011) 169–174.
[64] R. Gounder, M.E. Davis, AIChE J. 59 (2013) 3349–3358.
[65] Z. Qin, L. Lakiss, L. Tosheva, J.P. Gilson, A. Vicente, C. Fernandez, V. Valtchev, Adv. Funct. Mater. 24 (2014) 257–264.
[66] R. Gounder, M.E. Davis, J. Catal. 308 (2013) 176–188.